

Variable Pitch Reconstruction Using John's Equation

Başak Ülker Karbeyaz*, *Member, IEEE*, Ram C. Naidu, *Member, IEEE*, Zhengrong Ying, *Senior Member, IEEE*, Sergey B. Simanovsky, *Member, IEEE*, Matthew W. Hirsch, David A. Schafer, and Carl R. Crawford, *Fellow, IEEE*

Abstract—We present an algorithm to reconstruct helical cone beam computed tomography (CT) data acquired at variable pitch. The algorithm extracts a halfscan segment of projections using an extended version of the advanced single slice rebinning (ASSR) algorithm. ASSR rebins constant pitch cone beam data to fan beam projections that approximately lie on a plane that is tilted to optimally fit the source helix. For variable pitch, the error between the tilted plane chosen by ASSR and the source helix increases, resulting in increased image artifacts. To reduce the artifacts, we choose a reconstruction plane, which is tilted and shifted relative to the source trajectory. We then correct rebinned fan beam data using John's equation to virtually move the source into the tilted and shifted reconstruction plane. Results obtained from simulated phantom images and scanner images demonstrate the applicability of the proposed algorithm.

Index Terms—Advanced single slice rebinning (ASSR), computed tomography (CT), helical, John's equation, NSR, spiral, variable pitch.

I. INTRODUCTION

CONSTANT pitch helical cone beam (CB) computed tomography (CT) has been used for medical and security applications. The pitch is defined as the ratio of the table or conveyor displacement per gantry rotation divided by the height of the detector array along the axis of rotation (z) at isocenter. In certain applications, however, scanning at variable pitch is desirable. For example, in medical CT scanners, variable pitch reconstruction may be useful for scanning multiple organs in one helical scan or for tracking the bolus of injected contrast during angiography [1], [2]. In security CT scanners used for explosive detection [3], it is useful to slow down or stop the conveyor until the results of automated threat detection are available or increase the conveyor speed between bags to increase throughput.

Variable pitch algorithms have been developed as extensions of the Feldkamp algorithm [4], PI-line based reconstruction [5], [6], and exact 3-D reconstruction [7]. These methods employ computationally expensive cone-beam backprojection, i.e., backprojection along measurement rays. Therefore, they do not have the computational simplicity of 3-D reconstruction

algorithms based on 2-D rebinning such as advanced single slice rebinning (ASSR) [8]–[10]. The computational limitations justify a continuing investigation for faster but approximate 2-D rebinning algorithms which can readily be implemented in existing (very-large-scale integration) VLSI hardware. This warrants an extension of the ASSR algorithm to handle variable pitch reconstruction.

The ASSR algorithm rebins helical cone beam data into fan beam data, which are reconstructed into tilted slices that are interpolated into parallel slices. Since the source helix does not completely lie in the tilted reconstruction plane, the choice of fan data is approximate. In order to reduce the approximation error, Defrise *et al.* [10] showed that John's equation [11]–[13] can be used to compute a correction to the rebinned data to virtually move the source helix into the reconstruction plane to improve image quality.

To extend the ASSR algorithm to variable pitch, one would expect it to be sufficient to change the tilt angle of the slice plane to minimize the distance between the reconstruction plane and the halfscan segment of the varying source helix. However, this approach is not sufficient because the rays at the beginning and the end of the segment do not lie in the same plane and deviate in an asymmetric manner with respect to the center view in the halfscan segment. The corresponding reconstructed images show streak artifacts.

In this paper, we describe an algorithm called variable pitch ASSR (ASSR v) to reconstruct helical CB data by extending the ASSR algorithm as described in [14] and [15] to handle data acquired at variable pitch. In the ASSR v algorithm, we first compute rebinned data by applying the ASSR algorithm to the variable pitch data. The reconstruction planes used for rebinning are tilted and shifted relative to the source trajectory. We then use John's equation to compute a correction to the rebinned data, which moves the source virtually into the reconstruction plane. The correction is applied during rebinning using the method described by [10] with modification for variable pitch scanning.

We tested the ASSR v algorithm for medical applications using simulated variable pitch helical CB data of mathematical models of morphological phantoms. We also tested the algorithm for security scanners using simulated variable pitch helical CB data and data acquired by scanning bags on the COBRA checkpoint scanner manufactured by Analogic Corporation (Peabody, MA). In both cases, the reconstructed variable pitch images show image quality comparable to the images generated from constant pitch reconstructions. We therefore demonstrate the applicability of the proposed algorithm to reconstruct variable pitch data for the specific variable pitch profiles tested.

Manuscript received February 13, 2008; revised March 3, 2008. *Asterisk indicates corresponding author.*

*B. Ülker Karbeyaz is with Analogic Corporation, 8 Centennial Drive, Peabody, MA 01960 USA (e-mail: bkarbeyaz@analogic.com).

R. C. Naidu, Z. Ying, S. B. Simanovsky, and D. A. Schafer are with Analogic Corporation, Peabody, MA 01960 USA (e-mail: bkarbeyaz@analogic.com).

M. W. Hirsch is with The Media Laboratory, Massachusetts Institute of Technology, Cambridge, MA 02139 USA.

C. R. Crawford is with Csuptwo, LLC, Milwaukee, WI 53217 USA.

Digital Object Identifier 10.1109/TMI.2008.922689

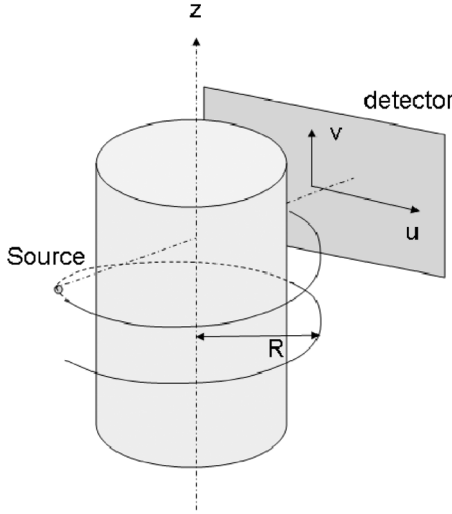


Fig. 1. Geometry of the acquisition system. The source travels on a helical trajectory of radius R along the z axis. The detector is defined by coordinates u and v .

II. BACKGROUND

A. Acquisition Geometry

Fig. 1 illustrates the data acquisition geometry that will be used in the algorithm description in the manner described by [10]. We denote $F(r)$ with $r = (x, y, z)$ as the smooth density function to be reconstructed. We measure CB projections for source vertices on the helical path $a(\lambda)$ oriented along the z axis

$$a(\lambda) = (R \cos \lambda, R \sin \lambda, f(\lambda)) \quad (1)$$

where λ is the view angle measured with respect to the x axis, and $f(\lambda)$ represents the source axial position during variable pitch data acquisition. Note that $f(\lambda)$ reduces to $h\lambda$ for constant pitch, where h is equal to source axial displacement per radian of gantry rotation and R is the source to isocenter distance. We consider a flat area detector, which moves with the cone vertex. We also assume that the detector coordinates are defined at isocenter, i.e., the detector array contains the z -axis and the source to detector distance is equal to R . We use cartesian coordinates (u, v) to locate the detector elements in the detector plane. These coordinates are defined by unit vectors e_u and e_v given by

$$e_u = (-\sin \lambda, \cos \lambda, 0) \quad (2a)$$

$$e_v = (0, 0, 1). \quad (2b)$$

We assume that the detector is large enough to avoid truncation of the projections along the u axis.

The CB projection data $g(u, v, \lambda, \zeta)$ for source position λ are defined as

$$g(u, v, \lambda, \zeta) = \int_{l_0(u) - \Delta l(u)}^{l_0(u) + \Delta l(u)} F(X(\lambda, u, l), Y(\lambda, u, l), f(\lambda) + lv + \zeta) dl \quad (3a)$$

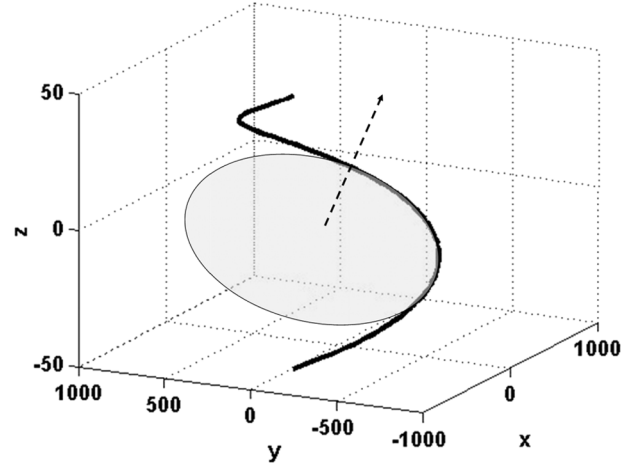


Fig. 2. Reconstruction plane chosen by ASSR. The solid line represents the source trajectory. The shaded ellipse represents the reconstruction plane, which is tilted to fit the source trajectory.

where

$$X(\lambda, u, l) = R \cos \lambda + l(-R \cos \lambda - u \sin \lambda) \quad (3b)$$

$$Y(\lambda, u, l) = R \sin \lambda + l(-R \sin \lambda + u \cos \lambda) \quad (3c)$$

$$l_0(u) = \frac{R^2}{R^2 + u^2} \quad (3d)$$

$$\Delta l(u) = \frac{\sqrt{(u_m^2 - u^2)(R^2 - R_{\text{FOV}}^2)}}{R^2 + u^2} \quad (3e)$$

where ζ is the axial displacement of the source-detector assembly (i.e., an axial shift of the ray at fixed orientation), R_{FOV} is the radius of the field-of-view (FOV) and $u \in [-u_m, u_m]$. Note that the measured helical cone beam data $g_{\text{cb}}(u, v, \lambda)$ are equal to $g(u, v, \lambda, \zeta = 0)$.

B. Advanced Single Slice Rebinning

The ASSR [9] is a method to reconstruct constant pitch helical cone beam data using 2-D backprojection. ASSR extracts segments of fan beam data from CB data. The fan beam data are chosen to lie on a tilted plane that is fit to the source helix. The fan data span an angular range known as a halfscan segment (ϕ), which is equal to $\pi + \delta$, where δ is the fan angle. The fan beam data are then reconstructed into tilted slices. The tilted slices are interpolated to obtain axial slices.

A schematic of the tilted plane chosen by ASSR is shown in Fig. 2. The plane is tilted about the central ray of the central view in the halfscan segment. For a halfscan segment of views acquired between $(-\phi/2, \phi/2)$, the plane is tilted about the x -axis. The equation of the tilted plane, which intersects with the helix at $\lambda = 0$, is given by

$$z = y \tan \eta \quad (4)$$

where the tilt angle η is chosen to minimize a cost function related to the average axial deviation between the rays and the tilted slice. The distance between the axial position of the source (source trajectory) and the axial position at which the reconstruction plane intersects the cylinder described by the source trajectory is shown in Fig. 3(a). The two curves intersect at three points, as described in [9].

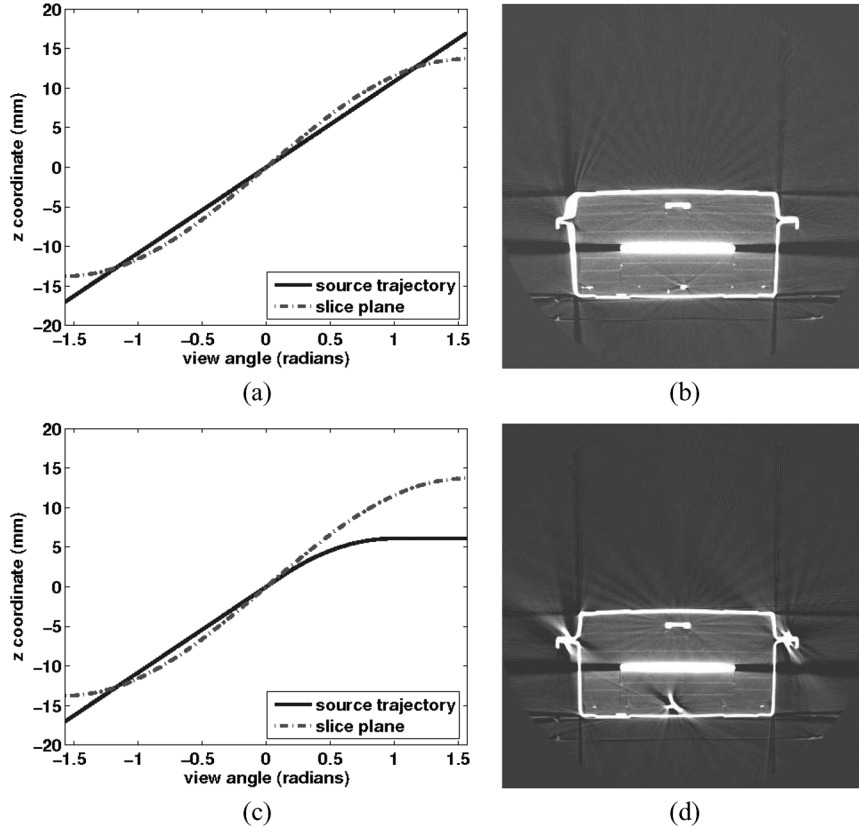


Fig. 3. Plot of the source trajectory and the reconstruction ellipse chosen by ASSR for constant pitch for (a) source moves at constant pitch (c) source moves at variable pitch. Images reconstructed with ASSR from (b) constant pitch data (d) variable pitch data.

A set of fan data is chosen from the cone beam data to approximate data that lie on the plane. The data are chosen to minimize the axial deviation of each ray from the tilted plane according to the equations described in the Appendix. For constant pitch reconstructions, the error due to the mismatch between the axial positions of the tilted plane and the source trajectory is maximum at the edges of the halfscan segment. In order to reduce artifacts caused by the edge mismatch, overscan correction is used during reconstruction [9], [16]. In overscan correction, additional views spanning an angle ϕ_{os} , are extracted along with the halfscan segment. During reconstruction, the last $N(\phi_{os})$ views, where $N(\phi_{os})$ is the number of views spanning the angle ϕ_{os} , are blended with data from the first $N(\phi_{os})$ views to reduce artifacts. The halfscan segment with overscan will be denoted as ϕ_h throughout the text and is equal to $\phi + \phi_{os}$.

C. Virtual Source Movement Using John's Equation

In order to reduce the distance between the reconstruction plane and the source trajectory, it is possible to correct the measured projection data to virtually move the source into the reconstruction plane, as shown by Defrise *et al.* [10]. The correction is possible because the cone beam projection data satisfy a consistency condition known, as John's equation [11]. The reader is referred to [10]–[12] for the mathematical details of the derivation of John's equation, the results of which are stated here without proof.

For constant pitch helical CT, the consistency condition on the weighted cone beam projections $g(u, v, \lambda, \zeta)$ is described by the following ultra-hyperbolic partial differential equation:

$$R^2 g_{u\zeta} - 2u g_v - (R^2 + u^2) g_{uv} = R g_{\lambda v} - R h g_{v\zeta} + u v g_{vv} \quad (5a)$$

where g_{xy} represents the partial derivatives of the projections g with respect to variables x and y . Following the derivation in [10], John's equation can be extended to variable pitch data acquisition using source axial positions defined by $f(\lambda)$ as follows:

$$R^2 g_{u\zeta} - 2u g_v - (R^2 + u^2) g_{uv} = R g_{\lambda v} - R f_\lambda g_{v\zeta} + u v g_{vv} \quad (5b)$$

where f_λ is the partial derivative of $f(\lambda)$ with respect to λ .

III. METHODS

A. Assumptions

In this paper, the following assumptions are made.

- 1) The detector array is sufficiently wide along the u direction so that projection data are not truncated.
- 2) The velocity of the conveyor belt or patient table can be varied continuously between zero and the velocity used for constant pitch data acquisition.
- 3) The patient table position or belt displacement is available during reconstruction.

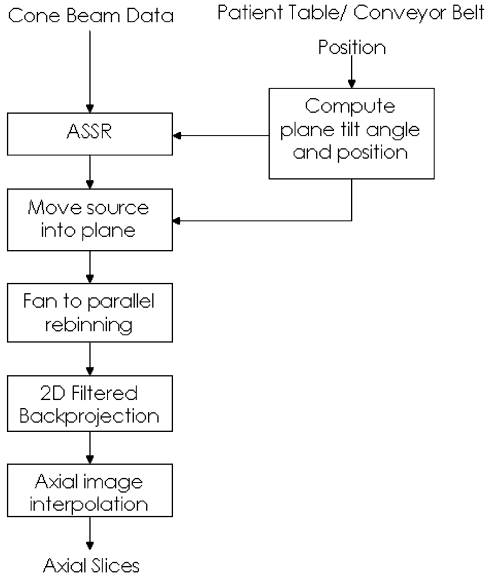


Fig. 4. Reconstruction flow diagram for ASSRv.

B. Overview of ASSRv

In the case of variable pitch, ASSR generates artifacts in the reconstructed images. The cause of the artifacts can be explained with respect to Fig. 3(c), which shows the axial position of the source for a variable pitch trajectory and the axial position at which the reconstruction plane intersects the cylinder described by the source trajectory. Note that the error between the reconstruction plane and source trajectory increases as the source decelerates and the two curves intersect at two points instead of three points and the chosen fan beam data when backprojected produce streak-like artifacts. The artifacts are evident when comparing the image reconstructed with ASSR from data acquired at constant pitch as shown in Fig. 3(b) with the image reconstructed with ASSR from data acquired at variable pitch as shown in Fig. 3(d) where the belt is stopped during acquisition.

To reduce the aforementioned artifacts, the ASSRv algorithm consists of the following steps applied to each halfscan segment of data that is reconstructed. The flow of the algorithm is shown in Fig. 4.

- 1) Calculate the tilt angle, and the position which define a reconstruction plane.
- 2) Correct the data to virtually move the source into the plane
 - a) compute the error between the plane and the source position;
 - b) compute partial derivatives of the projection data;
 - c) apply a correction with partial derivatives using John's equation extended to variable pitch data.
- 3) Reconstruct the data into tilted slices.
- 4) Axially interpolate the tilted slices to generate untilted slices.

The sections that follow present the detailed description of each of the above algorithmic steps.

C. Calculation of Reconstruction Plane

For constant pitch, the tilt angle η of the reconstruction plane is computed as described in [9]. For variable pitch, the reconstruction plane is specified for each half scan segment centered at a view angle λ_0 as follows. In addition to the optimum tilt angle (η_{λ_0}), we also compute the axial position offset of reconstruction plane relative to the axial position of the source in the central view of each halfscan segment (z_{λ_0}). These quantities are computed as functions of λ_0 as

$$(\eta_{\lambda_0}, z_{\lambda_0}) = \arg \min_{\eta, z_0} \int_{\lambda_0 - \frac{\phi}{2}}^{\lambda_0 + \frac{\phi}{2}} (\Psi)^2 d\lambda \quad (6a)$$

where the function Ψ is

$$\Psi = R \tan \eta \sin(\lambda - \lambda_0) + z_0 - \{f(\lambda) - f(\lambda_0)\} \quad (6b)$$

Equation (6a) minimizes the mean square error between the slice plane and source trajectory and is solved numerically for a given source trajectory to determine η_{λ_0} and z_{λ_0} .

D. Selection of Fan Beam Data From Cone Beam Data

For the tilted slice corresponding to λ_0 , the halfscan fan-beam data, $g^{\lambda_0}(u, \lambda)$, are estimated from the CB data, $g_{cb}(u, v, \lambda)$, acquired on the segment of the helix centered on $a(\lambda_0)$. Each ray is approximated by the equation of the ASSR algorithm

$$g^{\lambda_0}(u, \lambda) \approx g_{cb}(u, V_{\lambda_0}(u, \lambda), \lambda) \quad (7)$$

where the rebinning row function $V_{\lambda_0}(u, \lambda)$ is given by

$$V_{\lambda_0}(u, \lambda) = \tan \eta_{\lambda_0} (-R \sin \lambda_r + u \cos \lambda_r) + \left(\frac{R^2 + u^2}{R^2} \right) \{R \sin \lambda_r \tan \eta_{\lambda_0} + z_{\lambda_0} - f(\lambda) + f(\lambda_0)\} \quad (8)$$

where the relative angle $\lambda_r = \lambda - \lambda_0$. The detector row coordinate is chosen so that the measured ray intersects the rebinned row at a point P that lies closest to the z axis. The mathematical details of the calculation of $V_{\lambda_0}(u, \lambda)$ are described in the Appendix.

E. Data Correction Using John's Equation

The measured ray chosen by ASSR intersects the rebinned ray at a point that is closest to the z -axis. This point corresponds to a value of the integration variable l_0 in (3-D). In order to obtain exact rebinning, we must rotate the ray about the above intersection point until it lies within the tilted slice as follows. The source must move axially by $\Delta\zeta = R \sin(\lambda - \lambda_0) \tan \eta_{\lambda_0} + z_{\lambda_0} - (f(\lambda) - f(\lambda_0))$ and simultaneously the detector row coordinate must move by $-\Delta\zeta(u^2/R^2)$ as determined by the geometry of similar triangles. However, the detector array moves with the source cone vertex according to the definition of ζ in Section II-A. Therefore, a shift of $\Delta\zeta$ in source position also introduces a shift of $\Delta\zeta$ in detector array position. Therefore, the detector row coordinate must be shifted by a total displacement

of $-\Delta\zeta - \Delta\zeta(u^2/R^2)$, which is equal to $-\Delta\zeta(R^2 + u^2)/R^2$ to achieve exact rebinning.

As discussed in [10], these two shifts are equivalent to a rotation of the measured ray $(u, V_{\lambda_0}(u, \lambda), \lambda)$ in a vertical plane, until the ray is contained within the oblique slice. The corresponding fan beam data $g_J^{\lambda_0}(u, \lambda)$ are given by

$$g_J^{\lambda_0}(u, \lambda) = g(u, V_{\lambda_0}(u, \lambda) - \Delta\zeta(R^2 + u^2)/R^2, \lambda, \Delta\zeta). \quad (9)$$

The data $g_J^{\lambda_0}(u, \lambda)$ are obtained through a Taylor's series expansion of (9) around the measured data ($\zeta = 0$)

$$g_J^{\lambda_0}(u, \lambda) = g^{\lambda_0}(u, \lambda) + \Delta\zeta g_\zeta(u, V_{\lambda_0}(u, \lambda), \lambda, 0) - \Delta\zeta \left(\frac{R^2 + u^2}{R^2} \right) g_v(u, V_{\lambda_0}(u, \lambda), \lambda, 0) + O(\Delta\zeta^2) \quad (10)$$

In order to obtain the derivative of the data with respect to the variable ζ , we take the partial derivative of (10) with respect to the detector coordinate u to obtain

$$\begin{aligned} \frac{\partial g_J^{\lambda_0}(u, \lambda)}{\partial u} &= \frac{\partial g^{\lambda_0}(u, \lambda)}{\partial u} \\ &+ \Delta\zeta \left\{ g_{u\zeta} - \frac{2u}{R^2} g_v - \left(\frac{R^2 + u^2}{R^2} \right) g_{uv} \right. \\ &\quad \left. + \frac{\partial V_{\lambda_0}(u, \lambda)}{\partial u} \left(g_{v\zeta} - \frac{R^2 + u^2}{R^2} g_{vv} \right) \right\} \\ &+ O(\Delta\zeta^2). \end{aligned} \quad (11)$$

Inserting John's Equation (5b) into (11), we get

$$\begin{aligned} \frac{\partial g_J^{\lambda_0}(u, \lambda)}{\partial u} &= \frac{\partial g^{\lambda_0}(u, \lambda)}{\partial u} + \frac{\Delta\zeta}{R} \left\{ g_{\lambda v} - f_\lambda g_{v\zeta} + \frac{uv}{R} g_{vv} \right. \\ &\quad \left. + \frac{\partial V_{\lambda_0}(u, \lambda)}{\partial u} \left(g_{v\zeta} - \frac{R^2 + u^2}{R^2} g_{vv} \right) \right\} + O(\Delta\zeta^2). \end{aligned} \quad (12)$$

All of the partial derivatives with the exception of $g_{v\zeta}$ can be computed using measured data. We, therefore, approximate $g_{v\zeta}$ by g_{vv}/l_0 in (12), as described in [10]. Integrating (12) with respect to u , we generate improved rebinned data for variable pitch halfscan segments $|\lambda - \lambda_0| \leq \phi_h/2$ as

$$g_J^{\lambda_0}(u, \lambda) = g^{\lambda_0}(u, \lambda) + C_1 \int_{-\infty}^u du' \{ F_1 + C_2 F_2 \} \Big|_{v=V_{\lambda_0}(u', \lambda)} \quad (13a)$$

where C_1 , C_2 , F_1 , and F_2 functions are defined as

$$C_1 = \frac{R \tan \eta_{\lambda_0} \sin(\lambda_r) + z_{\lambda_0} - f(\lambda) + f(\lambda_0)}{R} \quad (13b)$$

$$F_1 = g_{\lambda v}(u', v, \lambda, 0) \quad (13c)$$

$$C_2 = \frac{R u' v - f_\lambda (R^2 + u'^2)}{R^2} \quad (13d)$$

$$F_2 = g_{vv}(u', v, \lambda, 0). \quad (13e)$$

Note that for simplicity of the notation the dependencies of C_1 , C_2 , F_1 and F_2 on u' , v , and λ are omitted. The u' integral is

computed as a weighted average of the integrals from the two boundaries $u = \pm u_m$ of the FOV, as described in [10]

$$\int_{-\infty}^u du' = \frac{u_m - u}{2u_m} \int_{-u_m}^u du' - \frac{u_m + u}{2u_m} \int_u^{u_m} du'. \quad (14)$$

Note that the algorithm described in this section is extended to cylindrical detector arrays, (γ, z) , through the detector mapping given by [9]

$$u = -R \tan \gamma \quad (15)$$

$$v = \frac{z}{\cos \gamma} \quad (16)$$

where γ is the angle subtended by the detector within the fan and z is the z -coordinate of the detector.

F. Derivative Computation

The correction of the data using John's equation requires the computation of the second derivatives of the projection data with respect to the projection view angle λ and the detector row v denoted by $g_{\lambda v}$ and g_{vv} , respectively. The derivatives are computed using the following steps. Let the location at which the derivatives are to be computed be denoted by (u, v, λ) . The projection data at locations (u, v_i, λ) , $i = 0, 1, 2$ where $v_0 < v \leq v_1 < v_2$ can be approximated using a Taylor's series expansion as follows:

$$g(u, v_i, \lambda, 0) = g(u, v, \lambda, 0) + (v_i - v) g_v(u, v, \lambda, 0) + \frac{(v_i - v)^2}{2} g_{vv}(u, v, \lambda, 0) \quad (17)$$

which is the standard 3 point finite difference discrete approximation using the first and second derivatives.

The partial derivatives g_v and g_{vv} can be obtained by solving (17) simultaneously using data from three consecutive samples in a single view, $i = 0, 1, 2$ where $v_0 < v \leq v_1 < v_2$.

Similarly, the mixed partial derivative $g_{\lambda v}$ is obtained by solving the equations

$$g_v(u, v, \lambda_j, 0) = g_v(u, v, \lambda, 0) + (\lambda_j - \lambda) g_{\lambda v}(u, v, \lambda, 0) \quad (18)$$

for two adjacent views $j = 0, 1$ where $\lambda_0 \leq \lambda < \lambda_1$.

To reduce artifacts introduced by high-frequency errors in the derivatives computed from sampled projection data, the data are filtered before computing the first and second derivatives with respect to v . This is achieved by convolving the data with a three-point triangular kernel applied along the v direction.

G. Image Reconstruction and Axial Interpolation

The data $g_J^{\lambda_0}(u, \lambda)$ are rebinned and reconstructed into tilted slices $I_{\text{tilt}}[i, j, k_{\text{tilt}}]$ using standard 2-D filtered backprojection [17], [18], where i and j are pixel coordinates, $0 \leq i < N_x$ and $0 \leq j < N_y$. The tilted slices are generated with a slice spacing of Δz .

During axial interpolation, the tilted slices are linearly interpolated to obtain axial slices $I[i, j, k]$ as follows. We assume

TABLE I
SIMULATION AND RECONSTRUCTION PARAMETERS

Parameter	Medical Scanner	Security Scanner
Source to isocenter distance (R) (mm)	621	575
Object translation for constant pitch per gantry rotation (mm) = $2\pi h$	30	68
Projections per rotation	960	720
Half fan angle $\frac{\delta}{2}$ (deg)	24	45
Tilt angle for constant pitch η (deg)	0.684	1.5
Detector width in z at isocenter	1.237	1.728
Number of rows	16	24
Scanner type	3 rd generation	3 rd generation
Detector array shape	Cylindrical detector array	Cylindrical detector array

that the axial slices are also generated at a slice spacing of Δz so that the k th axial slice has a z coordinate $z[k]$ equal to $k\Delta z$. The pixels in the k_{tilt} tilted slice have z -coordinates calculated as

$$z_{\text{tilt}}[i, j, k_{\text{tilt}}] = -x[i] \sin \lambda_0[k_{\text{tilt}}] \tan \eta_{\lambda_0[k_{\text{tilt}}]} + y[j] \cos \lambda_0[k_{\text{tilt}}] \tan \eta_{\lambda_0[k_{\text{tilt}}]} + z_{\lambda_0[k_{\text{tilt}}]} + k_{\text{tilt}} \Delta z \quad (19)$$

where $\lambda_0[k_{\text{tilt}}]$, $\eta_{\lambda_0[k_{\text{tilt}}]}$, and $z_{\lambda_0[k_{\text{tilt}}]}$ are the values of λ_0 , η_{λ_0} , and z_{λ_0} for the k_{tilt} tilted slice, $x[i]$ and $y[j]$ are the pixel coordinates calculated in millimeters with respect to isocenter given by

$$x[i] = \left(i - \frac{N_x - 1}{2} \right) \delta_p + x_0 \quad (20)$$

$$y[j] = - \left(j - \frac{N_y - 1}{2} \right) \delta_p + y_0 \quad (21)$$

where δ_p is the pixel size and x_0 and y_0 are x and y coordinates of the image center. The axial image $I[i, j, k]$ is then calculated as

$$I[i, j, k] = w[i, j, k] I_{\text{tilt}}[i, j, k_{\text{nn-tilt}}] + (1 - w[i, j, k]) I_{\text{tilt}}[i, j, k_{\text{nn-tilt}} + 1] \quad (22)$$

where $k_{\text{nn-tilt}}$ is the nearest tilted slice calculated as

$$k_{\text{nn-tilt}} = \max_{k_{\text{tilt}}} z_{\text{tilt}}[i, j, k_{\text{tilt}}] \leq z[k] \quad (23)$$

and $w[i, j, k]$ are linear interpolation weights calculated as

$$w[i, j, k] = 1 - \frac{z[k] - z_{\text{tilt}}[i, j, k_{\text{nn-tilt}}]}{z_{\text{tilt}}[i, j, k_{\text{nn-tilt}} + 1] - z_{\text{tilt}}[i, j, k_{\text{nn-tilt}}]} \quad (24)$$

as determined by the distance of each pixel in the axial slice from the neighboring tilted slices.

IV. TESTING AND RESULTS

We tested the ASSR v algorithm for medical applications using simulated variable pitch helical CB data for mathematical models of morphological phantoms and for security scanners using simulated variable pitch helical CB data and data acquired by scanning bags on the COBRA checkpoint scanner. The simulation and reconstruction parameters for both medical and security scanners are given in Table I.

A. Medical Application

1) *Simulated Data Generation*: The ASSR v algorithm was tested using simulated helical CB data generated for the modi-

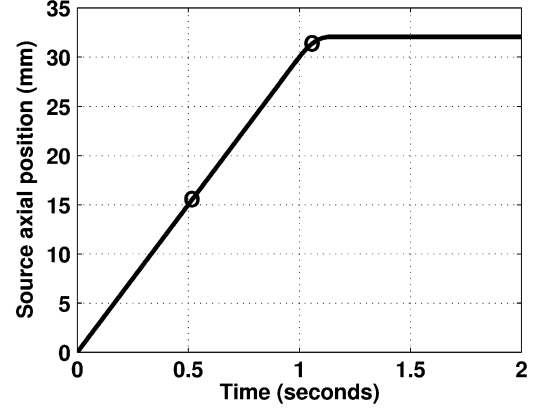


Fig. 5. Source axial position used to simulate variable pitch scanning of the head phantom on a medical scanner. The circles mark the slice locations for constant pitch and variable pitch reconstructions presented in Fig. 6.

fied version of the head phantom defined in [19]. The modification was done to exclude anatomical structures that were specified using clip planes, which cannot be handled by our simulation software. The data were simulated for the geometry of a 16 row medical CT scanner. The data were generated for the velocity profile shown in Fig. 5, where the phantom was moved at constant pitch for one rotation and then decelerated to zero within an angular range of 50° .

2) *Slice Sensitivity Profile*: The slice sensitivity profile (SSP) was measured using simulated helical CB data generated for two identical 0.3-mm-thick coins each centered on the scanner axis. Each coin was modeled in air with a diameter of 20 mm and a linear attenuation coefficient of $\mu = 2 \text{ cm}^{-1}$. The data were generated for the velocity profile shown in Fig. 5 where the circles mark the slice locations intersecting the centers of the coins. The overlapping images with an increment of 0.0625 mm were reconstructed with ASSR and ASSR v algorithms. For each image the mean CT value was measured in a $2 \text{ mm} \times 2 \text{ mm}$ region centered at isocenter. The variation of the mean value as a function of slice location was used to obtain the SSP. The full-width at half-maximum (FWHM) of the SSP was computed.

3) *Dose Utilization*: Following the definition in [9], the dose utilization is computed by calculating the fraction of the detector array that is covered by the intersection lines defined by (8). The dose was measured in the constant pitch and variable pitch regions for the slice locations marked by circles in Fig. 5.

4) *Results*: Fig. 6 shows axial images of the head phantom reconstructed with ASSR and ASSR v as follows. The top panels [Fig. 6(a) and (b)] show reconstructions of data obtained

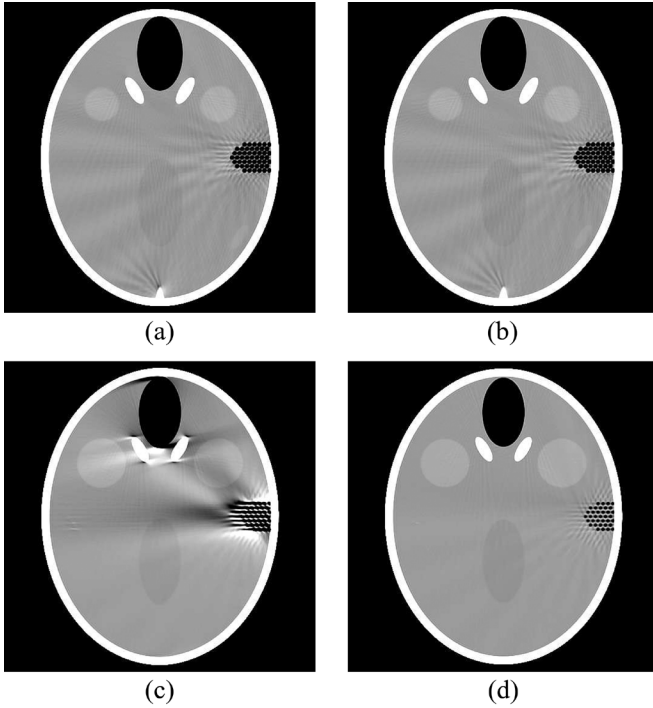


Fig. 6. Transaxial section of the head phantom reconstructed with the ASSR and ASSR v algorithms at slice locations specified in Fig. 5. (a) Constant pitch data reconstructed with ASSR. (b) Constant pitch data reconstructed with ASSR v . (c) Variable pitch data reconstructed with ASSR. (d) Variable pitch data reconstructed with ASSR v . The images are displayed with a window of 150 HU and a level of 35 HU.

by simulating constant pitch scanning. The bottom panels [Fig. 6(c) and (d)] show reconstructions of data obtained by simulating variable pitch scanning. The images are displayed with a window of 150 HU and a level of 35 HU.

At constant pitch (top panels), the image quality of the ASSR v reconstruction around petrous bone improves over ASSR in the manner described by [10]. When the pitch is decreasing during the scan, the images reconstructed with ASSR v have comparable image quality to the images reconstructed at constant pitch while the reconstruction of variable pitch using ASSR is degraded as visible in the region of inner ear and frontal sinus. The low-frequency windmill artifacts visible in Fig. 6(b) reduce as shown in Fig. 6(d) due to the increase in longitudinal sampling associated with reduced pitch [20].

At constant pitch, the FWHM value of the SSP for the ASSR algorithm is 1.61 mm. The corresponding FWHM value of the SSP measured in images reconstructed with the ASSR v algorithm from variable pitch data is 1.62 mm. This result shows that the difference in measured SSP between ASSR and ASSR v is less than 1%.

The dose is measured in the constant pitch and variable pitch regions for the slice locations marked by circles in Fig. 5. At constant pitch, the dose utilization is 99.2% for $\phi_{os} = 0.35$ radians. In the variable pitch region, the dose utilization is reduced to 43.1%.

B. Security Scanner

1) *Simulated Data Generation:* The ASSR v algorithm was tested using simulated helical CB data generated for the Turbell

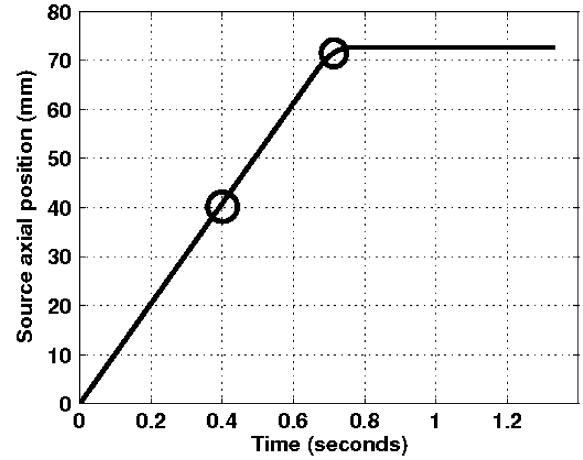


Fig. 7. Source axial position used to simulate variable pitch scanning of the Turbell clock phantom on security scanner. The circles mark the slice locations for constant pitch and variable pitch reconstructions presented in Fig. 9.

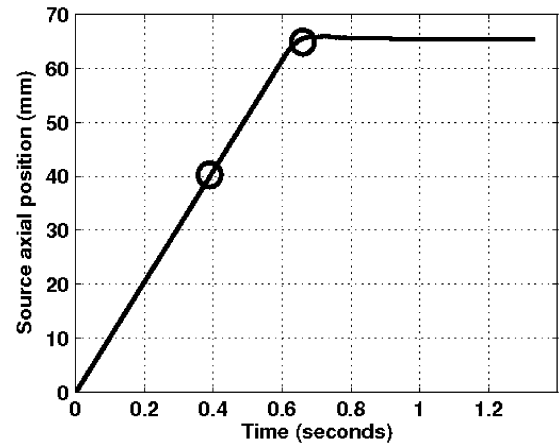


Fig. 8. Source axial position measured on the COBRA scanner during variable pitch scanning. The circles mark the slice locations for constant pitch and variable pitch reconstructions presented in Fig. 10.

clock phantom [21]. The data were simulated for the geometry of the checkpoint COBRA scanner described in Table I. The data were generated for the velocity profile shown in Fig. 7, where the phantom was moved at constant pitch for one rotation and then decelerated to zero in the second rotation within an angular range of 50° . The deceleration rate was chosen to simulate the deceleration of the conveyor belt on the COBRA scanner. To account for the differences between the FOV of the COBRA relative to a medical scanner, the dimensions of the clock phantom was scaled by a factor of three.

2) *Scanner Data Acquisition:* The ASSR v algorithm was also tested using data acquired by scanning bags on the COBRA scanner. To simulate scanning at variable pitch, the conveyor belt was stopped during the scan. The position of the conveyor was available in the raw data through an encoder that measures the conveyor speed. The conveyor position is shown in Fig. 8.

3) *Results:* Fig. 9 shows axial images of the Turbell clock phantom reconstructed with ASSR and ASSR v as follows. The top panels [Fig. 9(a) and (b)] show reconstructions of data obtained by simulating constant pitch scanning. The bottom panels

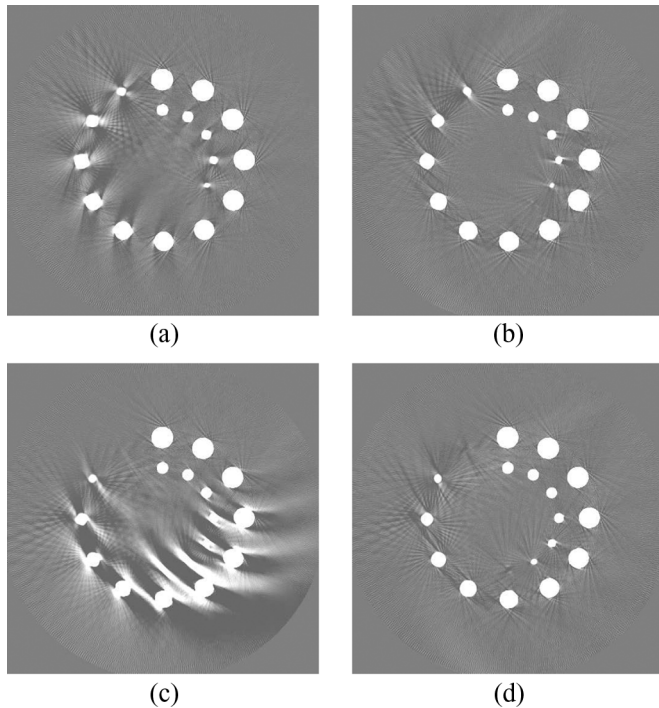


Fig. 9. Transaxial section of the clock phantom reconstructed with the ASSR and ASSR v algorithms on a security scanner at slice locations specified in Fig. 7. (a) Constant pitch data reconstructed with ASSR. (b) Constant pitch data reconstructed with ASSR v . (c) Variable pitch data reconstructed with ASSR. (d) Variable pitch data reconstructed with ASSR v . The images are displayed with a window of 256 HU and a level of 0 HU.

[Fig. 9(c) and (d)] show reconstructions of data obtained by simulating variable pitch scanning. The images are displayed with a window of 256 HU and a level of 0 HU.

At constant pitch (top panels), the image quality of the ASSR v reconstruction improves over ASSR in the manner described by [10]. When the pitch is decreasing during the scan, the images reconstructed with ASSR v have comparable image quality to the images reconstructed at constant pitch while the reconstruction of variable pitch using ASSR is degraded.

The corresponding results for scanner data are presented in Fig. 10. The images were obtained from the scan of an image quality phantom containing various objects. The section shown includes a metal comb at the top of the phantom, a central sheet object and a diagonal aluminum rod at the bottom. Again, the reconstruction of variable pitch data using ASSR v is comparable to the reconstruction of constant pitch data using ASSR. Note that streak artifacts are present in the image in the region of the sheet. These artifacts are not visible in simulations of the clock phantom and head phantom. We also verified that the artifacts are not visible in simulations of the sheet object used for testing. Therefore, the artifacts are not caused either by rebinning or by the reconstruction algorithm. The atomic number of the sheet object is intentionally chosen to be higher than the material for which the beam hardening correction is derived. We believe that the artifacts are caused by the insufficient correction for beam hardening of X-rays passing through the length of the sheet object.

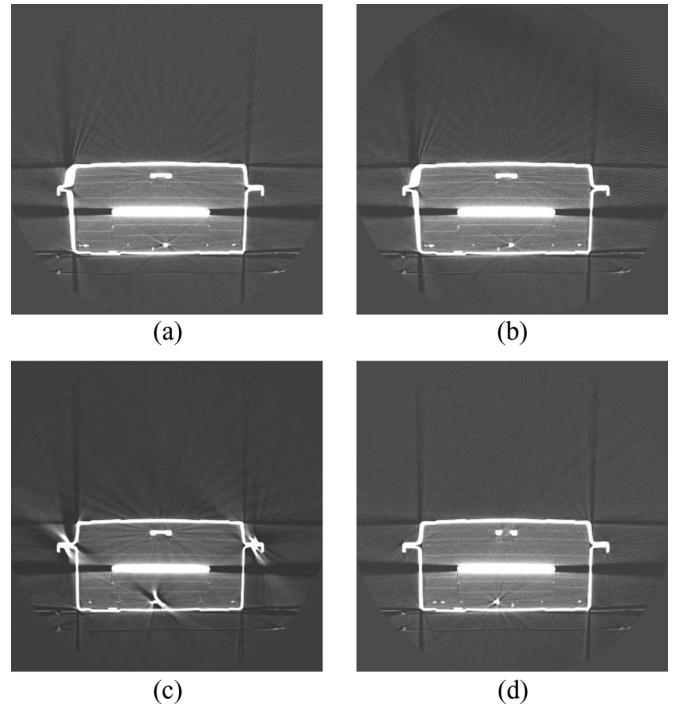


Fig. 10. Transaxial section of the image quality phantom reconstructed with the ASSR algorithm and ASSR v at slice locations specified in Fig. 8. (a) Constant pitch data reconstructed with ASSR. (b) Constant pitch data reconstructed with ASSR v . (c) Variable pitch data reconstructed with ASSR. (d) Variable pitch data reconstructed with ASSR v . The images are displayed with a window of 512 HU and a level of 0 HU.

V. DISCUSSION

We have demonstrated the feasibility of ASSR v to reconstruct images from helical cone beam data obtained at variable pitch. The current study was based on simulated phantom images and the data acquired from the COBRA checkpoint scanner. We have shown that at constant pitch, the image quality of the ASSR v reconstruction improves over ASSR in the manner described by [10]. When the pitch decreases during a scan, the images reconstructed with ASSR v have comparable image quality to the images reconstructed at constant pitch while the reconstruction of variable pitch using ASSR is degraded.

To extend ASSR for variable pitch scanning, intuitively one would assume that it is sufficient to vary the tilt angle of slice plane as a function of variable pitch rather than varying both the tilt angle and the axial offset of the plane with respect to the central view of each halfscan segment. A comparison of the slice planes chosen by both scenarios for a given source trajectory is shown in Fig. 11. When only the tilt angle is varied [Fig. 11(a)], the optimal slice plane may intersect the source trajectory only at the central view when compared with at least two intersections when the plane is chosen by optimizing both the tilt angle and axial offset of the slice plane [Fig. 11(b)]. The mean square error (MSE) between the source trajectory and the slice plane for each scenario is compared with that for constant pitch ASSR in Table II. The MSE values indicate that the slice plane chosen by optimizing both the tilt angle and axial offset is a better choice than the slice plane chosen by optimizing the tilt angle alone. This was verified by comparing images reconstructed on each of

TABLE II
 COMPARISON OF MEAN SQUARE ERRORS FOR SLICE PLANES CHOSEN FOR VARIABLE PITCH USING DIFFERENT OPTIMIZATION CRITERIA

Reconstruction	Data	Optimization	MSE	Error relative to constant pitch
Constant pitch	Constant pitch	Tilt Angle	1.4	1.0
Variable pitch	Variable pitch	Tilt Angle	6.5	4.6
Variable pitch	Variable pitch	Tilt Angle and Axial Position Offset	3.1	2.2

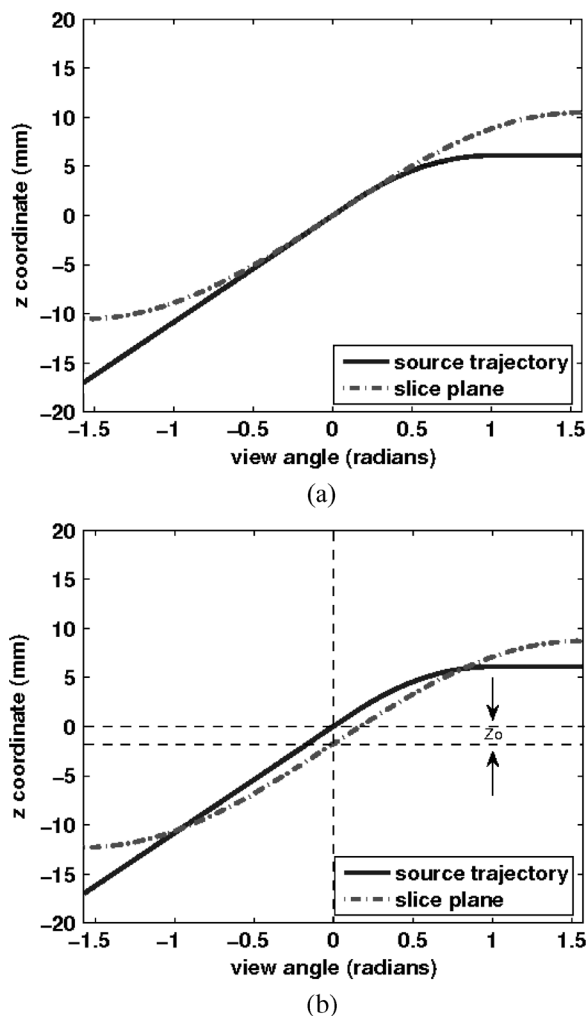


Fig. 11. Comparison of the slice planes chosen for a given variable pitch source trajectory by (a) varying the tilt angle of slice plane (b) varying both the tilt angle and the axial offset of the plane with respect to the central view.

the slice planes. Assuming that the MSE can be used as a measure indicative of the image quality of the reconstructed images, neither of the slice planes fit the source trajectory with the same MSE as the slice planes chosen for constant pitch. Therefore, in order to achieve image quality comparable to ASSR, it is necessary to apply the additional step of John's correction to the data. This correction allows the source trajectory to move into the reconstruction plane, which in turn reduces the MSE to be equal to or less than the MSE for constant pitch.

One of the limitations of the ASSR for medical CT is incomplete dose utilization for small pitch values [9]. Since we use the ASSR methodology to choose the rebinning row function on the detector array, the dose utilization of ASSR v is equivalent to ASSR algorithm. Future work includes extending ASSR v to more advanced rebinning methods such as [22], [23], which better utilize the detector area.

Variable pitch reconstruction is desirable on medical scanners for contrast enhanced CT angiography (CTA). CTA can be used to visualize blood flow in arterial and venous vessels throughout the body using a bolus of injected contrast. To achieve the best image quality, the data should be acquired when the intravascular concentration of contrast material is at its peak. To avoid misdiagnosis associated with scanning too early or too late relative to the arrival of peak concentration, the CT data acquisition must be individualized and optimized as described in [1]. However, these methods are limited because the table translation cannot be synchronized with the propagation of the bolus peak during constant pitch scanning. This misalignment causes image artifacts when the helical scanning speed is fast, contrast volume is small, and as well as when there are vessels from aneurysm formation or occlusive disease [1]. The use of a variable pitch offers the opportunity to synchronize the scanning aperture with the moving bolus peak for acquisition of data with maximized information [1], [2].

Variable pitch reconstruction is desirable on security scanners that scan baggage at airports. The reconstruction on security scanners built by Analogic Corporation assumes that data are acquired at constant pitch [8]. However, at airport checkpoints, where baggage is inspected, the time taken by screeners to resolve on-screen threats varies from bag to bag. On-screen threat resolution includes resolving threats detected by automatic explosive detection systems (EDS) and weapon detection algorithms and visually identifying prohibited items. A bag filled with objects may therefore require more time than the average time taken by operators to make a decision whether the bag should be manually searched. At an airport checkpoint, operators may therefore not be able to keep up with bag throughput at peak time. In the aforementioned situation, the operator may stop the conveyor belt in order to control access to bags while awaiting screener decision. When the belt is stopped, the images generated by the current reconstruction contain artifacts, as shown in Fig. 3. Since the artifacts can interfere with analysis by EDS, the scanner concept of operations requires that the conveyor backup and the bags be rescanned at constant pitch.

The process of backing up the conveyor and rescanning the bags reduces operational throughput. Variable pitch reconstruction allows the scanner to reconstruct images with acceptable image quality as the conveyor is slowing down or stopped. Assuming that one out of five bags is rescanned because the operator stops the conveyor belt, the use of variable pitch reconstruction allows a 20% increase in operational throughput by eliminating the need for conveyor backup and rescan. Additionally, variable pitch reconstruction can potentially allow an increase in conveyor speed between bags in order to increase throughput.

Future work includes extending the ASSR v algorithm to the Nutating Slice Reconstruction (NSR) algorithm. The ASSR [9] and NSR [8] algorithms are both methods to reconstruct constant pitch helical cone beam data into tilted slices using 2-D

backprojection. The difference between the ASSR and NSR algorithms lies in the method used to select fan beam data that lie on the tilted plane. In the case of ASSR, the fan data are chosen using an analytical expression that describes the intersection of the slice plane with the detector array. In the case of NSR, the interpolation table is derived from simulations. Given the computational simplicity of ASSR, we chose to extend the ASSR algorithm for variable pitch. Additional future work includes a comparative analysis of methods for axial resampling of the tilted slices, analysis of the sensitivity of the algorithm to errors in reported table speed, and real time implementation of ASSR v .

VI. CONCLUSION

ASSR v can be used to reconstruct helical cone beam CT data obtained at variable pitch. ASSR v combines the ASSR algorithm with a correction based on John's equation. Results obtained from simulated phantom images and scanner images demonstrate the applicability of the proposed algorithm for medical and security applications.

APPENDIX SELECTION OF FAN DATA

The fan data are selected to minimize the axial distance between the measured ray and the rebinned surface as described by [14]. The axial deviation, δz at position l along the fan beam ray (u, λ) is

$$\delta z(\lambda, u, l) = f(\lambda) - f(\lambda_0) + lV_{\lambda_0}(u, \lambda) - (y \tan \eta_{\lambda_0} + z_{\lambda_0}). \quad (25)$$

The quantity δz should be minimized over the range $\lambda \in [\lambda_0 - \phi_h/2, \lambda_0 + \phi_h/2]$, $u \in [-u_m, u_m]$ and $l \in [l_0(u) - \Delta l(u), l_0(u) + \Delta l(u)]$ which define the intersection of the ray with the limits of the field of view.

Following [14], we select the function V_{λ_0} , which minimizes a cost function Q that is equal to a weighted square of the axial deviation

$$Q(V_{\lambda_0}) = \int_{l_0(u)-\Delta l(u)}^{l_0(u)+\Delta l(u)} \frac{1}{l} (\delta z(\lambda, u, l))^2 dl. \quad (26)$$

Applying the constraint that $dQ/dV_{\lambda_0} = 0$, we get

$$V_{\lambda_0}(u, \lambda) = \frac{1}{2l_0(u)\Delta l(u)} \int_{l_0(u)-\Delta l(u)}^{l_0(u)+\Delta l(u)} \Theta dl \quad (27a)$$

where the function Θ is given by

$$\Theta = \tan \eta_{\lambda_0} (R \sin \lambda_r + l(-R \sin \lambda_r + u \cos \lambda_r) + z_{\lambda_0} - (f(\lambda) - f(\lambda_0))) \quad (27b)$$

where the relative angle $\lambda_r = \lambda - \lambda_0$. The (27a) can be solved to obtain the rebinning function

$$V_{\lambda_0}(u, \lambda) = \tan \eta_{\lambda_0} (-R \sin \lambda_r + u \cos \lambda_r) + \frac{R^2 + u^2}{R^2} \{R \sin \lambda_r \tan \eta_{\lambda_0} + z_{\lambda_0} - (f(\lambda) - f(\lambda_0))\} \quad (28)$$

Note that for constant pitch, $z_{\lambda_0} = 0$, and (28) reduces to the equation defined by ASSR [9], [14].

ACKNOWLEDGMENT

The authors would like to thank Dr. M. Defrise, Dr. S. Patch, and Dr. G. Gullberg for discussions of the application of John's equation to the ASSR algorithm, G. Larson for discussion of the NSR algorithm, C. Subramanian for collecting the data from the COBRA scanner, and Dr. D. Rozas for reviewing the manuscript.

REFERENCES

- [1] G. Wang and M. W. Vannier, "System and method of bolus chasing angiography with adaptive real time computed tomography CT," U.S. Patent 6 535 821, 2003.
- [2] Y. Ye, J. Zhu, and G. Wang, "Minimum detection windows, pi-line existence and uniqueness for helical cone-beam scanning of variable pitch," *Med. Phys.*, vol. 31, pp. 556–572, 2004.
- [3] Z. Ying, R. Naidu, and C. R. Crawford, "Dual energy computed tomography for explosive detection," *J. X-Ray Sci. Technol.*, vol. 14, pp. 235–256, 2006.
- [4] J. Hsieh and X. Tang, "Tilted cone-beam reconstruction with row-wise fan-to-parallel rebinning," *Phys. Med. Biol.*, vol. 51, pp. 5259–5276, 2004.
- [5] Y. Zou, X. Pan, D. Xia, G. Wang, and T. Jiang, "Exact image reconstruction in a helical cone-beam scan with a variable pitch," in *IEEE Nucl. Sci. Symp. Conf. Rec.*, Rome, Italy, 2004, vol. 7, pp. 4200–4203.
- [6] Y. Zou, X. Pan, D. Xia, and G. Wang, "PI-line-based image reconstruction in helical cone-beam computed tomography with a variable pitch," *Med. Phys.*, vol. 32, pp. 2639–2648, 2005.
- [7] A. Katshevich, S. Basu, and J. Hsieh, "Exact filtered backprojection reconstruction for dynamic pitch helical cone beam computed tomography," *Phys. Med. Biol.*, vol. 49, pp. 3089–3103, 2004.
- [8] G. L. Larson, C. C. Ruth, and C. R. Crawford, "Nutating slice CT image reconstruction apparatus and method," U.S. Patent 5 802 134, Sep. 1, 1998.
- [9] M. Kachelrieß, S. Schaller, and W. Kalender, "Advanced single-slice rebinning in cone-beam spiral CT," *Med. Phys.*, vol. 27, pp. 754–772, 2000.
- [10] M. Defrise, F. Noo, and H. Kudo, "Improved two-dimensional rebinning of helical cone-beam computerized tomography data using Johns equation," *Inverse Problems*, vol. 19, no. 6, pp. S41–S54, Dec. 1, 2003.
- [11] F. John, "The ultrahyperbolic equation with 4 independent variables," *Duke Math. J.*, pp. 300–322, 1938.
- [12] S. K. Patch, "Consistency conditions upon 3-D CT data and the wave equation," *Phys. Med. Biol.*, vol. 47, no. 15, pp. 2637–2650, 2002.
- [13] S. K. Patch, "Computation of unmeasured third generation VCT views from measured views," *IEEE Trans. Med. Imag.*, vol. 21, no. 7, pp. 801–813, Jul. 2002.
- [14] M. Defrise, F. Noo, and H. Kudo, "Rebinning-based algorithms for helical cone-beam CT," *Phys. Med. Biol.*, vol. 46, pp. 2911–2937, 2001.
- [15] M. Defrise, F. Noo, and H. Kudo, "Improved 2-D rebinning of cone-beam CT data using John's equation," in *Proc. IEEE Nucl. Sci. Med. Imag. Symp.*, 2002, pp. M10–M74.
- [16] C.R. Crawford and K.F. King, "Computed tomography scanning with simultaneous patient translation," *Med. Phys.*, vol. 17, pp. 967–981, 1990.
- [17] A. C. Kak and M. Slaney, *Principles of Computerized Tomographic Imaging*. New York: IEEE Press, 1987.
- [18] G. T. Herman, "Image reconstruction from projections," in *The Fundamentals of Computerized Tomography*. New York: Academic, 1980.
- [19] G. Lauritsch and H. Bruder [Online]. Available: <http://www.imp.uni-erlangen.de/forbild/english/results/head/head.html>
- [20] M. D. Silver, K. Taguchi, I. A. Hein, B. Chiang, M. Kazama, and I. Mori, "Windmill artifacts in multi-slice helical CT," in *Proc. SPIE*, M. Sonka and J. M. Fitzpatrick, Eds., 2003, vol. 5032, no. 1, pp. 1918–1927.
- [21] H. Turbell, "Cone beam reconstruction using filtered backprojection," Ph.D. dissertation, Univ. Linköping, Linköping, Sweden, 2001.
- [22] K. Stierstorfer, T. Flohr, and H. Bruder, "Segmented multiple plane reconstruction: A novel approximate reconstruction scheme for multi-slice spiral CT," *Phys. Med. Biol.*, vol. 47, no. 15, pp. 2571–2581, 2002.
- [23] T. Flohr, K. Stierstorfer, H. Bruder, J. Simon, A. Polacin, and S. Schaller, "Image reconstruction and image quality evaluation for a 16-slice CT scanner," *Med. Phys.*, vol. 30, no. 5, pp. 832–845, 2003.